ADVANCED PHOTONICS RESEARCH
Open Access
www.adpr-journal.com

Ultrahigh Sensitive Detection of Tau Protein as Alzheimer's Biomarker via Microfluidics and Nanofunctionalized Optical Fiber Sensors

Francesco Chiavaioli, Desiree Santano Rivero, Ignacio Del Villar,* Abián B. Socorro-Leránoz, Xuejun Zhang, Kaiwei Li, Enrique Santamaría, Joaquín Fernández-Irigoyen, Francesco Baldini, Daniel L. A. van den Hove, Lei Shi, Wei Bi, Tuan Guo,* Ambra Giannetti, and Ignacio R. Matias*

Alzheimer's disease (AD) is one of the most common neurodegenerative illnesses displaying the highest death rate in the elderly. However, the existing AD diagnostic system remains elusive due to lack of a technology that may ensure enough sensitivity and reproducibility, detection accuracy, and specificity. Herein, a straightforward approach is reported to realize lab-on-fiber (LoF) technology for AD biomarker detection based on a D-shaped single-mode fiber combined with nanometer-scale metal-oxide film. The proposed sensing system, which permits the generation of lossy-mode resonance (LMR), remarkably increases the evanescent field of light guided through the fiber, and hence the fiber-surrounding medium interaction. Moreover, such optical sensors are highly repeatable in results and can safely be embedded into a compact and stable microfluidic system. Herein, the specific detection of Tau protein (as one of the classical AD biomarkers that is highly correlated with AD progression) in a complex biofluid with a detection limit of 10^{-12} M and over a wide concentration range (10^{-3}–10 µg mL^{-1}) is successfully demonstrated. The proposed LoF biosensor is an appealing solution for rapid, sub-microliter dose and highly sensitive detection of analytes at low concentrations, hereby having the potential toward early screening and personalized medicine in AD.

1. Introduction

Maintaining physical and mental health in an aging society is of utmost importance. Alzheimer's disease (AD) is the most serious form of neurodegenerative disease. In fact, AD represents the most common cause of dementia, which has an estimated lifetime risk of about 20% for women and 10% for men,[1] while the global number of people estimated to be living with AD is expected to almost double every 20 years.[2] However, the only accurate diagnosis is through postmortem neuroanatomical analysis. Therefore, accurate antemortem diagnosis is urgently needed for early detection of AD to empower reliable estimation of prognosis, intervention, and monitoring of the disease.

The overall situation has reiterated a need that has always haunted physicians: to prevent the progression of the disease in time, or at least to slow it down, if not yet possible to cure it. There are classic routes to do this, but they are not 100% accurate. On the one hand, one makes use of an extensive neuropsychological and neurological examination. On the other hand, one has access to laboratory methods to detect altered proteins in the cerebrospinal fluid (CSF) combined with neuroimaging (magnetic resonance imaging [MRI], positron tomography, etc.). Neuroimaging, although more objective, is time-consuming and expensive, with still a certain degree of uncertainty.[3] The powerful and straightforward advantage of biomarkers may be the ease of use and low cost, so unique

F. Chiavaioli, F. Baldini, A. Giannetti
Institute of Applied Physics "Nello Carrara" (IFAC)
National Research Council of Italy (CNR)
50019 Sesto Fiorentino, Italy
E-mail: f.chiavaioli@ifac.cnr.it

The ORCID identification number(s) for the author(s) of this article can be found under https://doi.org/10.1002/adpr.202200044.

DOI: 10.1002/adpr.202200044

D. Santano Rivero
Department of Electrical and Electronic Engineering
Public University of Navarra
31006 Pamplona, Spain

I. Del Villar, A. B. Socorro-Leránoz, I. R. Matias
Department of Electrical and Electronic Engineering and Institute of Smart Cities (ISC)
Public University of Navarra
31006 Pamplona, Spain
E-mail: ignacio.delvillar@unavarra.es

features to be employed in the early screening of AD. Luckily, more recently, many steps have been made and research has increasingly focused on organic biomarkers, i.e., altered proteins (Tau protein [Tau] and amyloid-beta [Aβ]) that accumulate from the beginning of the physio-pathological process, long before symptoms appear.[4–7] Their aggregates are detectable in CSF well before clinical manifestations. Specifically, the increase in Tau level provides above all the real warning signal for the onset of AD,[8] capable also of distinguishing the risk of different stages of dementia since it correlates with disease progression as recently indicated.[9] Tau derives from alternative mRNA splice variants that originate from a single gene and result in mature proteins that vary in size from 352 to 441 amino acids, and hence with a molecular weight from 36.8 to 45.9 kDa, respectively. In the human brain, alternative splicing of mRNAs results in six molecular isoforms that are highly hydrophilic, and hence soluble and heat stable.[10] Tau-441 is the largest size human brain Tau with a total of 441 amino acids in length,[11] and hence the large number of amino terminal inserts enhances its binding to tubulin, which makes Tau-441 the most effective in promoting microtubule assembly. Moreover, with Tau-441 being the longest Tau isoform, it has also the largest number of phosphorylation sites and so far represents one of the most effective and clinically relevant Tau protein.[12]

Traditional methods for Tau detection are mostly based on enzyme-linked immunosorbent assay (ELISA) or, more recently, on mass spectrometry.[13] While ELISA possesses the well-known disadvantages of labeled methods in comparison with label-free ones (i.e., tedious assay procedure, time-consuming, and reagent-consuming approach), mass spectrometry is costly, needs a skilled technician, cannot be integrated into a portable system and, most importantly, is unable to differentiate among molecule isomers with the same charge-to-mass ratio. Different biological fluids are being used to detect Tau, such as CSF, serum, plasma, and blood.[4,14] Level of Tau in CSF has been shown to increase in the very early stages of the disease where its elevated level makes higher the risk of a quicker development of AD dementia. Still, only the quantification of Tau through brain imaging (using positron emission tomography) or in CSF has been considered the gold standard method for patient stratification and as an enrollment criterion for clinical trials for AD.[15,16] In fact, the Tau level in other biofluids at the early stage of the disease is extremely low (down to pg mL^{-1}) which requires supersensitive techniques to the detriment of accuracy, specificity, and repeatability in the detection. Despite standard procedures for CSF collection (e.g., lumbar puncture) are generally highly invasive, sometimes risky and painful for the patient, specific and reliable detection of Tau in CSF as AD biomarker continues to be a major challenge due to the unreliability and complexity of the results in case of blood. Therefore, the added value of developing a science-enabled, effective, and highly sensitive photonic platform capable of accurate, label-free, and real-time monitoring and quantification of Tau levels in CSF is very necessary but still challenging.

Optical sensors are a class of sensors that have attracted growing attention in cutting-edge applications over the last years, such as for monitoring both the environmental conditions toward green and sustainable economy and health parameters in a personalized fashion.[17–19] Among them, fiber-optic sensors permit to exploit the fascinating and peculiar light control at unprecedented and outstanding levels, together with other inherent features, which other optical technologies can hardly attain.[20–22] In all cases, the interaction of light traveling within the photonic device with the surrounding environment generates surface waves (for instance, evanescent waves, Bloch waves, surface plasmon polaritons, waves related to lossy/leaky mode or derived from guided mode, etc.), that are able by the evanescent field to assess every change occurring in the surrounding medium through the measurement of refractive index (RI).[23] Given the particular coupling of light, these photonic devices mainly feature the presence of resonance (i.e., attenuation dip or absorption peak) in their transmission or reflection spectrum that changes its optical properties as a function of surrounding RI. Generally, micro/nano lab-on-fiber (LoF) sensing platforms, together with nanoparticles, nanofilms, or nanostructures, allow tailoring the light–matter interaction with remarkable resolution, precision, and accuracy, thus envisaging advanced technological-level optical platforms with ultrahigh performances.[24]

Herein, we report a highly sensitive, specific, and reproducible application of real-time and noninvasive detection of Tau at low levels exploiting LoF technology.[25] We demonstrate that there is

A. B. Socorro-Leránoz, I. R. Matias
Bioengineering group at IdiSNA
Navarra Institute for Health Research
31008 Pamplona, Spain

X. Zhang, K. Li
Institute of Photonics Technology
Jinan University
Guangzhou 510632, China

E. Santamaría, J. Fernández-Irigoyen
Clinical Neuroproteomics Unit
Navarrabiomed, Hospital Universitario de Navarra (HUN)
Public University of Navarra and Navarra Institute for Health Research
31008 Pamplona, Spain

D. L. A. van den Hove
Department of Psychiatrie and Neuropsychologie
School for Mental Health and Neuroscienc, Faculty of Health
Maastricht University
6211 LK Maastricht, Netherlands

L. Shi
JNU-HKUST Joint Laboratory for Neuroscience and Innovative Drug Research
Jinan University
Guangzhou 510632, China

W. Bi
Department of Neurology
The First Affiliated Hospital of Jinan University
Guangzhou 510632, China

T. Guo
Institute of Photonics Technology
Jinan University
Guangzhou 510632, China
E-mail: tuanguo@jnu.edu.cn

T. Guo
Southern Marine Science and Engineering Guangdong Laboratory (Zhuhai)
Zhuhai 519000, China

a clear relationship between the level of Tau and the measured changes in the optical features of surface waves excited on the fiber surface by means of lossy-mode resonance (LMR). For any biochemical changes occurring around the fiber surface, the associated modification of the surface RI has a very strong impact on the optical features of the LMR, which is reflected in the measured transmission spectrum of the sensor.[23] LMR pinpoints improved detection flexibility and several advantages over well-established optical technology platforms based on other resonance-based phenomena,[26] such as a relatively easy tunability of the resonance wavelength over a wide spectral range from visible to near infrared (NIR) as a function of the coating thickness, the possibility of exciting both transverse electric (TE) and magnetic (TM) polarization states of light, and the capability of multiple LMR generation.[27] The combination of a special geometry of single-mode fibers, i.e., a D-shaped configuration, with additional nanometer-scale metal-oxide coating to support LMR, has offered remarkable results in terms of the limit of detection (LOD) of biomolecules in real samples.[21] Since tin dioxide (SnO_{2-x}) guaranteed an extremely high RI sensitivity in comparison with other LMR-generating nanomaterials,[26,28] this material has been used in the present study.

2. Results

2.1. Sensor Characterization and Imaging

Several LMR-based optical fiber sensors coated with SnO_{2-x} have been manufactured to conduct this study. **Figure 1**a details the 3D sketch of the nanofunctionalized optical fiber sensor for the detection of biomolecules. The presence of a nanometer-scale metal-oxide film allows the generation of LMR,[26] and the sensing mechanism relies on the evaluation of RI changes occurring in the fiber surface[23] and determined by the LMR spectral shift (Figure 1b). The spectrum of some devices is shown in Figure S1a, Supporting Information. It can be observed that the spectral position (i.e., wavelength) as well as the visibility (i.e., the depth) of the LMR can vary in the NIR region, but the LMR keeps a high visibility (18–28 dB) and an average bandwidth of 25 nm. In order to assess the impact of the repeatability and reproducibility of the entire manufacturing process on the sensing performance, a numerical analysis has been conducted (Supporting Information) by studying the RI sensitivity of the proposed sensor. The LMR spectral shift in short (1350 nm) and long (1550 nm) wavelength ranges as a function of the surrounding medium RI is detailed in Figure S1b, Supporting Information. Comparable values of RI sensitivity (maximum error of 15%) with respect to the state of the art[26,28,29] are achieved (Supporting Information), thus ensuring very similar penetration depth of the LMR-related evanescent field, and hence comparable sensing performance is securely envisaged. Overall, the RI sensitivity of those devices is generally higher than other optical fiber sensors or grating-based configurations[29,30] and averages around 4–8 μm^{-1} RIU,[31] with a sensitivity record of 14 μm^{-1} RIU.[21]

The used samples have been characterized by different imaging tools, such as high-resolution scanning electron microscopy (SEM; Apreo S, Thermo Fisher Scientific, USA) and atomic force microscopy (AFM; BioScope Catalyst, Bruker, USA). The processing software used in the analysis of SEM and AFM images is Phenom ParticleX AM Desktop SEM and NanoScope Analysis, respectively. **Figure 2**a,b detail SEM images of the LoF sensor cross section of one sample at low magnification of 1300× and 5000×, respectively. From these images, it is possible to observe the D-shaped form of the optical fiber sensor used in this study. Moreover, the outer portion that surrounds the fiber sample and is brighter than the remaining area represents the SnO_{2-x} nanocoating. In order to completely characterize the proposed sensor, high magnification (40 000×) images have been taken considering samples at three different stages during Tau detection: sample 1 refers to the optical fiber sensor coated with SnO_{2-x} and then functionalized with a polymeric layer (Eudragit L100); sample 2 accounts for sample 1 further coated with a biological layer represented by the immobilization of the anti-Tau antibody (biological recognition element, BRE) onto the fiber surface; finally, sample 3 refers to sample 2 further coated with another biological layer represented by the plateau of the assay after the interaction with a saturating Tau concentration. Figure 2c,e,g detail high magnification SEM images of

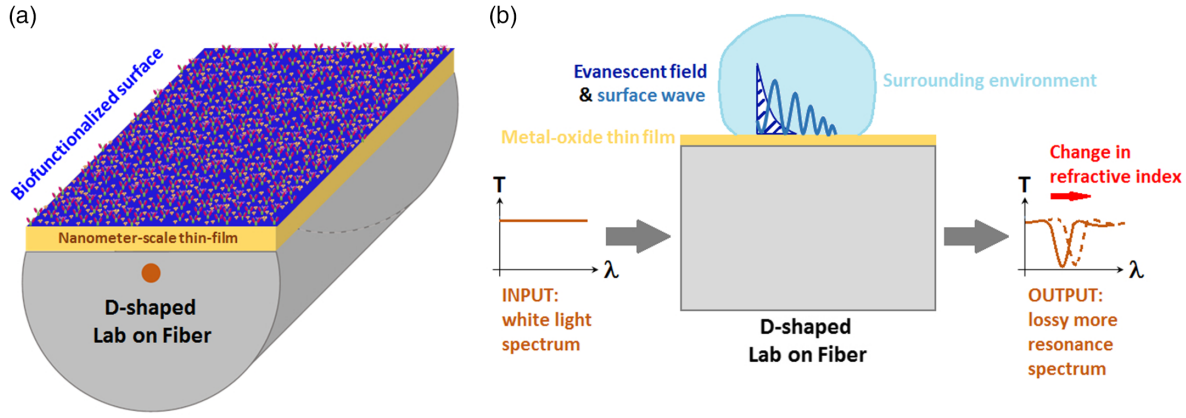

Figure 1. a) 3D view of the nanofunctionalized D-shaped lab-on-fiber sensor. b) Related sensing mechanism based on the evaluation of refractive index changes, through evanescent wave interaction, that occur in the fiber surface and are determined by the spectral shift of the LMR, which is generated by a metal-oxide thin film.

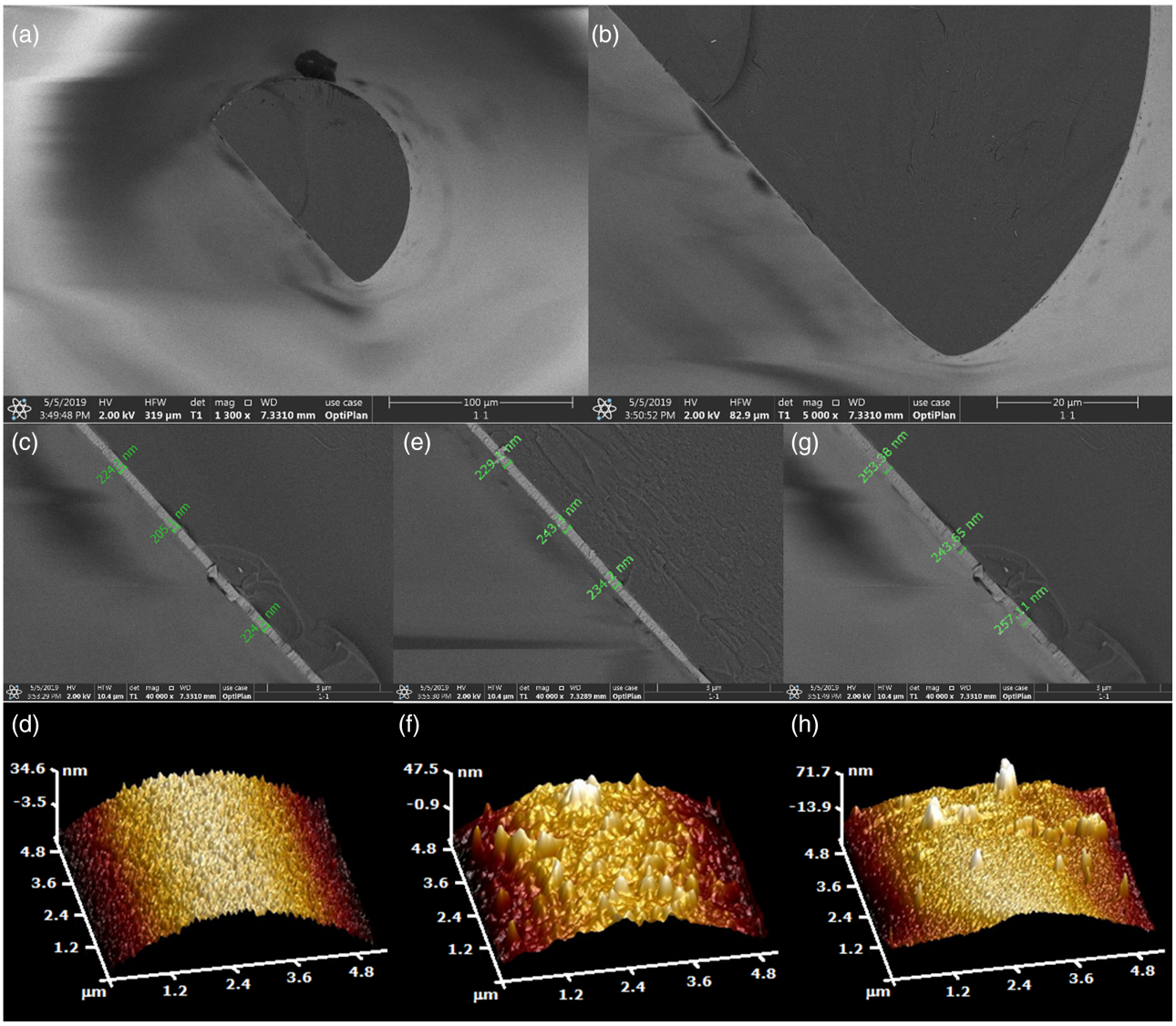

Figure 2. SEM images of the cross section of nanofunctionalized D-shaped fiber sensor at low magnification of a) 1300× and b) 5000×. High magnification (40000×) SEM and 5 × 5 μm^2 scan area size AFM images considering samples at three different stages during Tau detection: sample 1 coated with SnO_{2-x} and polymeric layer (c, SEM; d, AFM), sample 2 further coated with a biological layer of anti-Tau antibody (e, SEM; f, AFM), and sample 3 further coated with another biological layer of Tau analyte at the end of the assay (g, SEM; h, AFM).

the optical fiber sensor cross section of samples 1, 2, and 3, respectively. From these images, it is possible to determine the thickness of the entire nanocoating that has been evaluated with the integrated SEM software tool (×T microscope Server). All the values are gathered in **Table 1**. It can be observed that the average thickness of a uniform bio-layer of antibodies is confirmed to be roughly (16 ± 7) nm as already reported in the literature.[32]

With AFM, for a complete characterization of the samples, different sizes of the scan area are used ranging from 1.1 × 1.1 μm^2 up to 10 × 10 μm^2. Here, the AFM images refer to an intermediate value of 5 × 5 μm^2 for the size of the scan area. The root mean square (rms) roughness has been extrapolated with the integrated AFM software tool (NanoScope Analysis) from Figure 2d for sample 1, from Figure 2f for sample 2, and from Figure 2h for sample 3. All the values are gathered in Table 1. It is important to notice that the surface roughness as well as the overall nanocoating thickness increase as a function

Table 1. SEM and AFM imaging parameters of interest for nanofunctionalized optical fiber sensors.

Type of imaging	Sample 1	Sample 2	Sample 3
SEM (40 000× magnification)	Nanofunctionalized film thickness [nm]		
	218 ± 9	235 ± 6	251 ± 6
AFM (5 × 5 μm^2 scan area size)	Surface roughness, rms [nm]		
	15.7	16.3	24.9

of the complexity of the biological layer with a progressive reduction in surface flatness, starting from the polymeric layer up to the complete assay at increasing concentrations of Tau, passing by the immobilization of the BRE onto the fiber surface. This gives evidence of the effectiveness and reliability of the implemented assay for Tau detection. The complete AFM analysis with smaller and larger sizes of the scan area is provided in Supporting Information (Table S1 and Figure S2, Supporting Information).

2.2. Assay Optimization and Specificity Assessment

After the optical characterization of the samples, the assay for the detection of Tau level has been envisaged. In doing this, two key aspects have to be considered in order to improve the sensor specificity and accuracy (hence, the repeatability of the assay):[33] the first encompasses the selection of the blocking agent for surface passivation, while the second concerns the selection of a biofluid for Tau detection in real scenario.

To answer to the first point, different blocking agents have been tested individually and in combination: bovine serum albumin (BSA), ethanolamine (EA), and tris-hydrochloric acid (Tris-HCl). In case of BSA, two standard concentrations diluted in phosphate-buffered saline (PBS) solution were used: 1% and 0.1%. The detailed analysis of this point is provided in Supporting Information. By looking at Figure S3 and S4, Supporting Information, BSA represents one of the best options for blocking action together with surface passivation, as expected when antibodies are grafted onto the biosensing layer surface of optical sensors. Particularly, 0.1% BSA is selected in this study given its response with an average shift of the LMR wavelength of roughly (2.5 ± 0.5) nm and further confirmed thanks to a low unspecific response, as discussed in the following paragraph. All the results are plotted in **Figure 3**a.

The possibility of using this optical fiber technology in real scenarios is underpinned by developing an approach where the biomarker under investigation is present in a real and complex matrix, such as serum, blood plasma, CSF, and not in a simple buffer like PBS. Therefore, Tau has been spiked first in human serum as complex matrix. However, the results (Figure S5, Supporting Information) clearly detail that nonspecific attachment of biomolecules occurred when human serum was used as biofluid, confirmed by a large shift of the LMR wavelength, notwithstanding the use of BSA as blocking agent. Moreover, differently from the sensing mechanism of LMR-based device,[34] the signal decreases when Tau spiked in 1:10 diluted serum at specific concentrations (up to $1\ \mu g\ mL^{-1}$) is injected (Supporting Information). This undoubtedly demonstrates the ineffective and inefficient detection of Tau by using the proposed assay. In contrast, BSA is routinely used and proved as efficient blocking agent of free functionalities when antibody-based binding interactions are featured in complex matrices.[34,35] The achieved results in human serum could turn out that, by spiking Tau in serum, a greater difficulty, and hence a less probability for the analyte to reach the BRE occurs due to a more intense electric charge effect over the biomolecules and/or to a denser matrix. In general, the transport of target molecules to the sensing surface that is an interplay between diffusion, convection, and interaction plays a key role as the biochemical reaction itself in governing binding kinetics, and, ultimately, the performance.[36] Another reason could stem from the fact that CSF has a slightly lower pH (7.28–7.32) than other biofluids (7.35–7.45). The change of the biological matrix, associated with this slightly different pH, could change the inherent nature of biomolecules and antibodies (less hydrophilic and more hydrophobic for instance).[37] This would imply a change in the conformation of biomolecules, resulting in the aggregation of antibodies and then in a worse detection capability.[38] Anyway, according to the literature[5,7,9] and the developed surface functionalization involving the surface passivation with BSA, Tau was spiked in CSF as the biofluid for AD biomarker assessment.

Undiluted commercially available CSF has been used first. However, repeated ($n > 3$) experiments have shown that the LMR baseline exhibited a redshift (i.e., spectral shift toward longer wavelengths) before and after the injection of CSF and the trend reached the equilibrium in subsequent injections with great reduction in magnitude (Figure S6, Supporting Information). Even if the value of the signal change is dramatically less than that achieved with human serum (one-seventh on average), there is still a clear indication of weak biomolecule attachment onto the fiber surface, confirmed by the typical

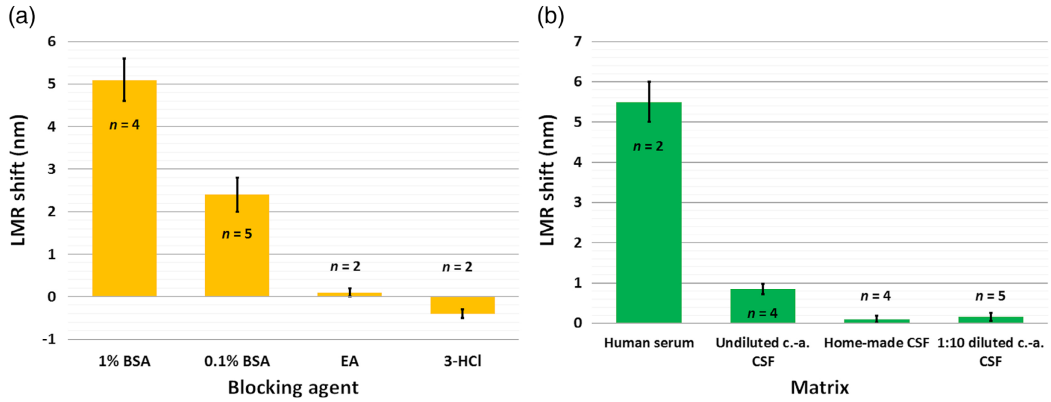

Figure 3. Analysis of the response of nanofunctionalized optical fiber sensors to repeated (n) experiments considering a) different blocking agent solutions in surface passivation, such as bovine serum albumin at 1% and 0.1%, ethanolamine, and tris-hydrochloric acid, and b) different biofluids where the target analyte is spiked, such as human serum, undiluted and 1:10 diluted commercially available CSF, and homemade CSF.

kinetics of interaction (i.e., the exponential behavior). This could stem from the presence of a very low level of proteins in the biofluid. A custom-made CSF was prepared (Experimental Section) to mimic the saline part of brain CSF. Now, the signal exhibited a variation (<0.1 nm) comparable within the signal noise (0.08 nm) in repeated experiments ($n > 3$), which is one-tenth of the previous case on average (Figure S7, Supporting Information). This clearly demonstrates a very good specificity, since any attachment of biomolecules (any kinetics of interaction is also shown) occurs when custom-made Tau-free CSF is used. However, this was expected, since this solution mimicking the real biofluid consists just of different types of salts without any added protein.

Conversely, for the development of an effective and reliable device toward future early screening of AD, a biofluid that mimics as much as possible the real scenario had to be taken into account. To address this, the commercially available CSF was used with a standard 1:10 dilution in PBS. Dilution of complex biofluids (1:10 or even 1:100) that surely requires a further preconditioning step in real scenario is routinely carried out for the assessment of biosensing platforms,[39] but it does not have an impact on the sensing performance since Tau concentration, which is spiked in the sample, remains unchanged. In this case, the signal exhibits just a slight increase of the baseline (0.15 nm on average in repeated experiments, $n > 3$). A very weak biomolecule attachment onto the fiber surface still happens, but the specificity has been improved due to dilution. Therefore, 1:10 PBS-diluted commercially available CSF has been finally selected to conduct this study with the Tau spiked in. As shown in Figure 3b, the LMR shifts caused by homemade CSF and 1:10 diluted commercially available CSF are comparable, and this proves that there is a negligible interaction between the biosensing layer on the fiber surface and any of the biological compounds contained in the commercially available CSF. All the results assessing the assay specificity are showed in Figure 3b.

2.3. Tau Detection

The selected Tau, i.e., Tau-441, is the longest of Tau isoforms and consists of 441 amino acids with molecular weight of 45.9 kDa. After the proper surface nanofunctionalization and immobilization of the antibody, a wide range of Tau concentrations of clinical interest was tested from 1 ng mL^{-1} (21.8 pM) to 10 µg mL^{-1} (218 nM).[40,41] As previously discussed, 1:10 PBS-diluted commercially available CSF was used as real biofluid in repeated experiments where Tau was spiked, instead of serum which revealed to be not a suitable biofluid (Figure S8, Supporting Information). **Figure 4** accounts for the complete implementation and related assessment of the nanofunctionalized fiber sensor when the Tau-441 was spiked in 1:10 PBS-diluted CSF. The developed assay consists of the first steps for the preparation of the sensing bio-layer (Figure 4a) and then of the second steps where different increasing concentrations of target analyte are detected (Figure 4b). By repeating several times ($n = 5$) the same assay with different sensors and by plotting the average of subsequent (15–20) measurements for each analyte concentration, the biosensor dose–response curve is drawn as shown in Figure 4c. The gray line accounts for the sigmoidal fit of the experimental points by means of the Logistic function

$$\lambda_{LMR}(C_{Tau}) = \lambda_{LMR,min} + \frac{\lambda_{LMR,max} - \lambda_{LMR,min}}{\left(1 + \left(\frac{C_{Tau}}{C_{Tau,0}}\right)^{-h}\right)^{s}} \quad (1)$$

where $\lambda_{LMR}(C_{Tau})$ represents the actual LMR wavelength, $\lambda_{LMR,min}$ (signal at the blank sample) and $\lambda_{LMR,max}$ (signal at the highest Tau concentration) are the minimum and maximum LMR wavelengths (i.e., the values corresponding to the horizontal asymptotes), respectively, h and s are two coefficients related to the slope of the sigmoidal curve, C_{Tau} and $C_{Tau,0}$ account for the actual Tau concentration and the one equal to 50% of the total dynamic range of the LMR optical signal, respectively. The function used is formally equivalent to the Langmuir isotherm and represents a well-accepted mathematical model that quantifies the degree of interaction between ligand binding sites.[42] The error bar is also showed in black; when it is not displayed, this means that the standard deviation σ is less than the symbol size of the experimental point. For the sake of completeness, when a slow dissociation rate constant occurs testified by the strong antibody–analyte interaction, an accumulation effect due to serial injections of analyte concentrations certainly influences the number of available binding sites onto the functionalized fiber surface. This outcome which is more evident and not negligible at high analyte concentrations has to be taken into account when the dose–response curve of the biosensor is drawn and used to determine the analyte concentration of an unknown sample. However, mass coverage of the BRE is largely abundant with respect to the concentrations injected; a 20-fold higher concentration of BRE with respect to the highest Tau protein concentration was used. In addition, it is worth underlining that, despite serial injections are performed, it is possible to determine the binding constants (association and dissiociation constants above all) from the dose–response curve of affinity-based biosensors simply by using the "kinetic titration" approach.[43] Figure 4d reports on the specificity test that confirms the detailed analysis given in the previous section, where a very small change in the optical signal (LMR wavelength) <0.2 nm occurs when the used biological matrix is injected. The response is also confirmed when the injection of diluted CSF is performed in two distinct and consecutive cycles (Figure S6b, Supporting Information). The shift of the LMR wavelength in case of the lowest Tau concentration is almost threefold greater than that of 0-spiked analyte solution, thus testifying the remarkable specificity.

The assessment of the performance of the nanofunctionalized LoF technology platform is carried out with complete statistics by collecting all the results achieved using different sensors and plotting a selection of them considering the outliers. Data have been scaled down to the mean value of the LMR wavelength at 0-spiked analyte solution (i.e., optical signal at the baseline without any Tau protein spiked in), and hence the new parameter is named $\Delta\lambda_{LMR}$. **Figure 5** details the median and mean values, the Gaussian distribution of the experimental data, and the interquartile range (IQR) for the lower Tau concentrations using Origin software (OriginLab, OriginPro 2020). To complement the statistical analysis, GraphPad Prism v7.00 software is also used. The three data groups, referring to the 0-spiked Tau

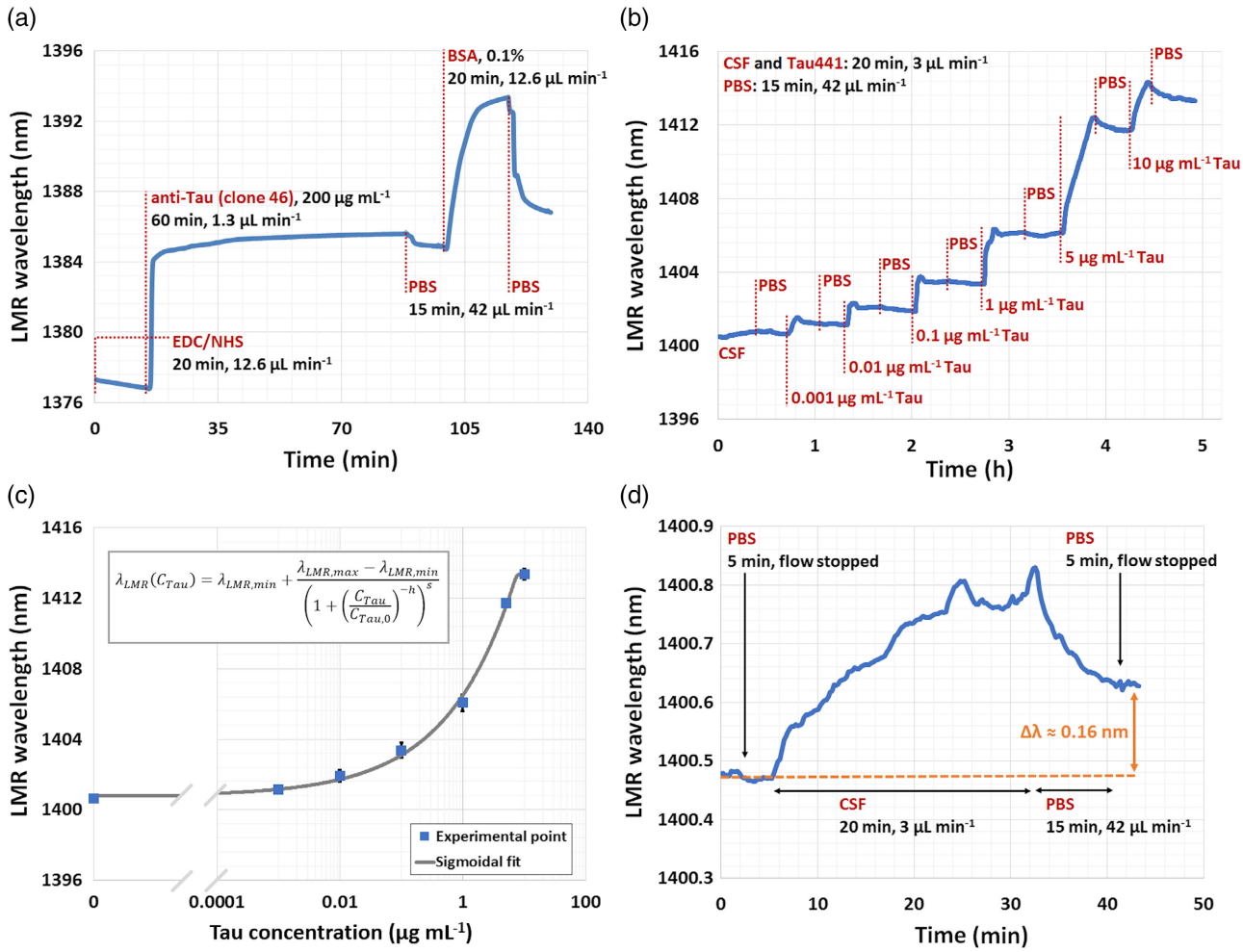

Figure 4. a) Preparation of the sensing bio-layer by grafting the Tau antibody (anti-Tau, clone 46) onto nanofunctionalized fiber sensor. b) Detection of Tau analyte (Tau-441) spiked in 1:10 PBS-diluted CSF biofluid in concentrations ranging from 1 ng mL^{-1} to 10 µg mL^{-1}. c) Biosensor dose–response curve in repeated ($n = 5$) experiments, together with the fitting function used in the gray box. d) Specificity test accounting for the optical signal change when 0-spiked analyte solution is injected representing the used biological matrix, i.e., 1:10 PBS-diluted CSF.

concentration (blank measurements) and the two lower Tau concentrations, are further analyzed with a one-way analysis of variance (ANOVA) test and with Tukey's honest significant difference test. Asterisks showed in Figure 5 indicate the statistical significance among the measurements where the symbol "****" means a p-value < 0.0001 (p-values greater than 0.05 are considered not significant), thus reporting an overall excellence significance. Two crucial and practical parameters have been taken into account to better determine the sensor performance: LOD and limit of quantification (LOQ) defined as 3σ and 10σ of the blank measurement (i.e., the optical signal related to 0-analyte solution), respectively.[23,44] An LOD of 2.4 pM (110 pg mL^{-1}) and an LOQ of 25 pM (1.15 ng mL^{-1}) were attained. It is worth underlining that Figure 5 gathers the results obtained with different LMR-based D-shaped fiber sensors in repeated experiments. The different values for each concentration, that is to say the variance of experimental results, account not only for the reproducibility issue of LMR-based D-shaped fiber sensors but also for the repeatability in the assay implementation.

For the sake of completeness and to facilitate future translation of the proposed research into feasible solutions, the obtained results have been compared using undiluted commercially available CSF as real biofluid (Supporting Information). Figure S9, Supporting Information, details the sensorgram, the specificity test, and the biosensor dose–response curve by repeating the same assay ($n = 4$) and by plotting the average of subsequent (15–20) measurements for each analyte concentration. All the achieved results are gathered in **Table 2** for a direct comparison.

To complement our workflow, affinity and specificity analysis were performed combining different proteomics-based biochemical approaches, such as Western blotting (WB) and ELISA. All the details on the methodology and procedures are provided further ahead in Experimental Section/Methods, while the results are presented in Figure S10, Supporting Information.

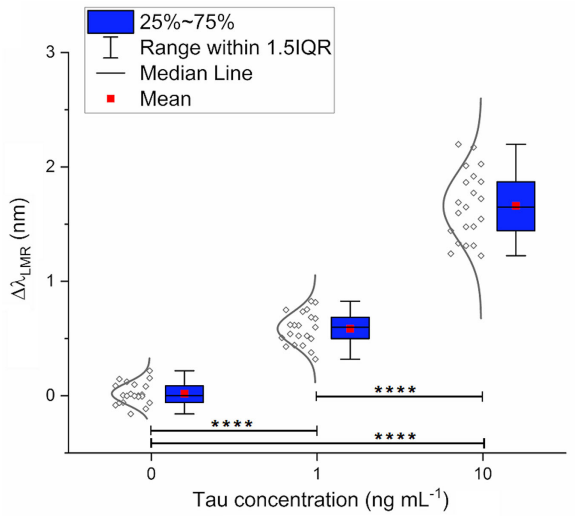

Figure 5. Complete statistics of all nanofunctionalized fiber sensors in the low Tau concentration range for the performance assessment using Origin software, and ANOVA and Tukey's honest significance difference tests.

Table 2. Performance assessment of nanofunctionalized fiber sensors for tau detection using diluted and undiluted matrices.

Type of biofluid	Tau concentration range [ng mL^{-1}]	Total signal change [nm]	Blank σ [nm]	LOD [pM]	LOQ [pM]
1:10 PBS-diluted CSF	1–10^4	13.23	0.038	2.4	25
Undiluted CSF	10–10^4	13.79	0.045	3.23	37

A LOD of 500 ng mL^{-1} was obtained using an ELISA kit. WB revealed multiple bands with different molecular weights in Tau samples as shown in Figure S10, Supporting Information. The standard molecular weight of Tau-441 is 45.9 kDa as we used in the developed assay protocol. However, its molecular weight increases up to roughly 67 kDa as observed by WB due to the capability of such isoform to self-interact and hence to create a dimer or intermediate forms in a sodium dodecyl sulfate-polyacrilamide gel electrophoresis (SDS-PAGE) gel.[45] Overall, these data revealed that the proposed assay featured a biological setup that partially mimicked the toxicity induced by Tau oligomers in the context of AD.[46]

Finally, to assess the potential reusability of the proposed biosensing platform, a preliminar regeneration test is performed following a similar protocol already tested for the regeneration of antibody–antigen–based biosensor by using 1% w/v SDS diluted in PBS as regeneration solution.[21] Three consecutive regeneration cycles are carried out. The results are detailed in Figure S11 and Table S2, Supporting Information. It is worth pointing out that SDS works well in case of antibody–antigen interactions, with a good recovery of the baseline and almost repeatable signal change when a fixed low concentration of analyte is injected. The expected outcomes at higher analyte concentrations are not trivial to predict, although the regeneration process strongly depends on the regeneration solution and protocol, when the antibody–analyte affinity and the involved Van der Waals forces of molecules have already been considered in advance.

3. Discussion and Conclusion

Over the last years, a lot of efforts have been made to determine Tau structure as a way to understand Tau function and its mechanisms of action.[47] However, these efforts have primarily based on traditional biochemistry and molecular biology approaches. Novel optical methods allow the exploitation of the fascinating and peculiar light management at unprecedented levels, which other optical technologies can hardly attain.[20,21] The interaction of light traveling within the photonic sensor with the surrounding environment exploits electromagnetic waves (for instance, evanescent waves, Bloch waves, and surface plasmon polaritons) that are able to assess every change occurring in the surrounding medium.[23] Micro/nanotechnology, together with nanoparticles, nanofilms, or nanostructures in general, permit to tailor such surface waves with outstanding spectral resolution, precision, and accuracy, thus envisaging high-performance and high-technological-level optical platforms. Here, we show that it is possible to effectively and reliably quantify the level of Tau in CSF by using nanofunctionalized LoF optical sensors embedded into custom-made developed microfluidics. The sensing system exploits a recent, high-performance and super versatile physical phenomenon termed LMR, which is similar to surface plasmon resonance (SPR) in terms of mathematical description of electromagnetic fields,[48] but distinct in terms of the optical features from other well-investigated optical approaches, such as SPR, fiber gratings, and interferometry, with potentially remarkable advantages over the other optical detection approaches in terms of resonance tunability, sensitivity, figure of merit, and multiparameter sensing.[26,27] An elaborate fundamental study has showed the huge potentiality of LMR technology able to attain sensitivity in the order of tens of μm RIU^{-1} and resolution below 10^{-7} RIU in aqueous environments.[49] Furthermore, in the proposed sensing system that has been envisaged by embedding the fiber within an ad hoc developed microfluidics,[30] the variation in the optical features of light depends solely on the changes in the RI of surrounding medium and not on other sources of noise like fiber deformation, temperature fluctuations, polarization effects (light polarization is fixed once LMR has been optimized), or source power fluctuations (wavelength-based detection is used). The deposition of nanomaterials onto the fiber sensing region (i.e., SnO_{2-x} in this case) permits not only to excite the LMR but also to improve the light–matter interaction in the fiber surrounding medium, thus allowing to attain remarkable limits of detection of biomolecules down to pM and fM range in repeated and independent experiments.[21,26] Overall, the entire fabrication process of the sensor did not affect the structural integrity of the fiber, hence ensuring the sensor robustness and reproducibility.

The progress on AD and related biomarker studies are making very quick progress in the last years, with the continued discovery of novel biomarkers.[50] Among them, some studies reported the analysis and characterization of the ratio between different biomarkers, such as phosphorilated Tau (pTau), total Tau (tTau or

simply Tau), and Aβ.[51–53] However, it is still not clear which of them could be considered the new gold standard for the diagnosis of AD at the early stage, given also the possible overlap with other neurodegenerative diseases, such as Creutzfeldt–Jakob disease (CJD).[54] Overall, the level of Tau in CSF from AD patients exceeds 1 ng mL^{-1} (≈22 pM) in comparison with controls or other neurodegenerative diseases, such as Parkinson's disease, where the Tau concentration is below 1 ng mL^{-1},[40,41] even if other studies suggest a lower cutoff value of 195 pg mL^{-1} (≈4.2 pM) for Tau detection in CSF of AD patients.[55] Here, we clearly prove with LODs below both these previously reported clinical levels that the proposed sensing system possesses all the characteristic features, such as high sensitivity, high specificity, repeatability, and reproducibility, to be used in the label-free detection of AD biomarkers by simply selecting an AD biomarker (Tau-441) with confirmed clinical relevance in CSF, as a proof of concept for its applicability on easy and early diagnosis of AD. The relationship between the sensor response and the level of Tau protein at low concentrations (below 0.1 μg mL^{-1}) is found to be highly reproducible, as also testified by the preliminary reusability results attained when a regeneration test was carried out (Supporting Information). Moreover, the attained LOQs, which are very close to the previous clinical levels, demonstrate once more that nanofunctionalized LoF sensors represent a credible and feasible biosensing technology platform to be used in real scenario of biochemical and biomedical applications. In this context, the results attained using an undiluted biological matrix that are comparable with the diluted case (Table 2) are of primary importance. In fact, since any dilution is required, this can speed up the analysis and assessment of the sample taken from a patient and hence can considerably increase the applicability of the sensing platform to a real scenario. Overall, despite the issue of serial injections of analyte concentrations without regeneration between two consecutive samples that leads to a reduced availability of number of capturing elements at the fiber surface and hence to a conservative estimation of the performances (LOD, LOQ, and dynamic range), the proposed advanced biophotonic platform enables to detect Tau protein concentrations of clinical interest, thus surely below nM or 0.1 μg mL^{-1}, in a robust, reliable, and reproducible manner. Results are further complemented by complete statistical analysis. In addition, the label-free quantification in the proposed model assay is an undoubtedly simpler, more flexible, cheaper, and less time-consuming when compared to a label-based approach.[56] Meanwhile, the ELISA method based on an in-house assay was used to benchmark our sensing system. The ELISA experimental results indicate an LOD of 7.5 nM (500 ng mL^{-1}), which is about three orders of magnitude greater than that attained with the proposed sensing platform (with both undiluted and 1:10 PBS-diluted CSF), thus indicating once more the remarkable performance. Obviously, there are commercially available ELISA kits which detect Tau in the low pg mL^{-1} range, as well as the proposed biosensing platform. However, none of them use the same pair of selected antibody–antigen, and hence the results would be difficult to compare, mainly due to standardization issues and primary antibodies used, which might impact on the performances (LOD and specificity).

Currently, the literature reports just one paper where an SPR-based optical fiber sensing system was described for the detection of Tau.[57] Despite the claimed performances are better than those here reported, it should be underlined that the procedure for attaining the LOD was not detailed and any noise analysis and statistics were performed. Moreover, when the achieved results were compared with real samples, the error bar is comparable with the optical signal, thus testifying a low reliability and repeatability of the results. Overall, considering more general optical sensing systems that do not make use of fibers directly, there is still a limited number of published articles in the field. All those consist of chip-based sensors where different optical approaches are used for the detection of Tau, such as bio-layer interferometry combined with aptamers,[58] multi-spot localized SPR,[59] and single-molecule array (SIMOA) as an ultrasensitive but also very complex technology.[60] As a future perspective, it is worth mentioning the possibility of implementing supersensitive assays with optical fibers in order to further improve the sensor performance,[61] even if repeatability and reproducibility still represent a big challenge to be faced.

4. Experimental Section

Principle and Characteristics of LMR-Based Nanofunctionalized LoF Sensors: It is well known that SPR occurs when the real part of the thin film permittivity is negative and higher in magnitude than both its own imaginary part and the permittivity of the material surrounding the thin film (i.e., the optical waveguide and the surrounding medium in contact with the thin film). Conversely, LMR occurs when the real part of the thin film permittivity is positive and higher in magnitude than both its own imaginary part and the permittivity of the material surrounding the thin film.[26,34] Therefore, LMRs are achieved using materials with low imaginary part (i.e., absorption or extinction coefficient, k) and high real part (i.e., RI, n) of the complex refractive index (CRI), such as metallic oxides and polymers, instead of the noble metals typically used in SPR devices.[26,29] This agrees well with the mode transition phenomenon, closely related to the LMRs in the sense that a mode guided in the optical fiber experiences a transition to guidance into the thin film with losses, which leads to a coupling of light transmitted from the fiber to the thin film.[62] The result is a reduction of the transmitted power in a specific wavelength range, where the LMR is then located. For this reason, contrary to SPR, LMR can be excited for both TE- and TM-polarized light.[26,34] Moreover, the central wavelength of the LMR can be easily tuned in the optical spectrum by controlling the film thickness,[26,34] thanks to the fact that many metallic oxides present a rather constant *n* in a wide range of wavelengths. This is not possible with the materials that generate SPR or localized SPR. In addition, if the film thickness is further increased, more LMRs can be generated, leading to a multiresonance platform that can be exploited for multiparameter sensing.[27] As far as the sensitivity to the surrounding medium RI is concerned, it has been successfully proved that LMR presents better performance than SPR.[63] Overall, the choice of the correct material is crucial for attaining good sensing performances. One of the key rules is to increase the real part of the CRI of the thin film for improving the sensitivity to the surrounding medium RI,[34] a parameter that is usually a good indicator of the biosensing performance. The role of fiber geometry also plays an important role in the improvement of performance. However, LMRs are typically broader than SPRs, though the D-shaped fiber has been proved as the best structure for facing this issue.[26] At the same time, the use of D-shaped fiber permits to separate the TE and TM components of light polarization, which avoids the limitation in certain cases that TE and TM components overlap each other in the optical spectrum.[49] Following these rules, a remarkable LOD in the detection of immunoglobulin G was obtained with SnO_{2-x} as thin film and D-shaped single-mode fiber as LMR-based photonic platform working in the NIR range. This photonic platform permitted to track wavelength shifts of the first LMR (the most sensitive LMR[34]) in the telecommunication C-band,

where the sensitivity was also enhanced when compared to the visible region.[23]

The 3D sketch of the nanofunctionalized D-shaped fiber is shown in **Figure 6**a, together with the model assay used for the detection of Tau protein using antibodies as BRE. The sensor cross section is presented in Figure 6b, while the related intensity distribution of the optical field of the fundamental core mode ($HE_{1,1}$) is depicted in Figure 6c. Numerical analysis was also performed using FIMMPROP, an integrated module of FIMMWAVE that is a highly flexible waveguide CAD tool based on fully vectorial mode solvers. By following a workflow similar to a previous publication and using the same parameters for the optical fiber and the nanometer-scale films (i.e., SnO_{2-x} and Eudragit polymer),[21] a distance of 5 μm between the fiber core and the D-shaped fiber surface was considered in the numerical analysis carried out for the evaluation of RI sensitivity (Figure S1b, Supporting Information) and the intensity distribution of the optical field of $HE_{1,1}$ mode. The finite element method (FEM) solver was used for the evaluation of the second feature, with a mode profile resolution of 400 in both *x* and *y* axes, and with 100 elements per diagonal in the grid. In this case, the cross-sectional energy density of the electromagnetic wave of $HE_{1,1}$ is showed in Figure 6d. It can be observed a spike on the right side that defines the D-shaped region of the fiber cladding (≈5.25 μm radius) with respect to the fiber core (≈4.05 μm radius). Figure 6e details the enlargement of $HE_{1,1}$ energy density at the interface between the D-shaped region of the fiber and the surrounding medium with special attention to the tail of the evanescent field (red highlighted). The sensing principle sketched in Figure 6f relies on the monitoring of LMR wavelength shift in the transmission spectrum of the fiber. When this sensing parameter is displayed in real time (i.e., the sensorgram), it allows studying the kinetics of binding interactions (association and dissociation constants). Moreover, when the signal change is plotted as a function of the analyte concentration (i.e., the dose–response curve), it permits to extrapolate a series of parameters of interest for any biosensor, such as LOD.

Fabrication of LMR-Based Nanofunctionalized LoF Sensors: The present optical sensor is based on the wavelength shifts of an LMR generated by the deposition of a SnO_{2-x} thin film onto a D-shaped single-mode fiber. Standard single-mode fibers (Corning SMF-28) with a cladding/core diameter of 125/8.2 μm were used to obtain the sensing substrate. They were

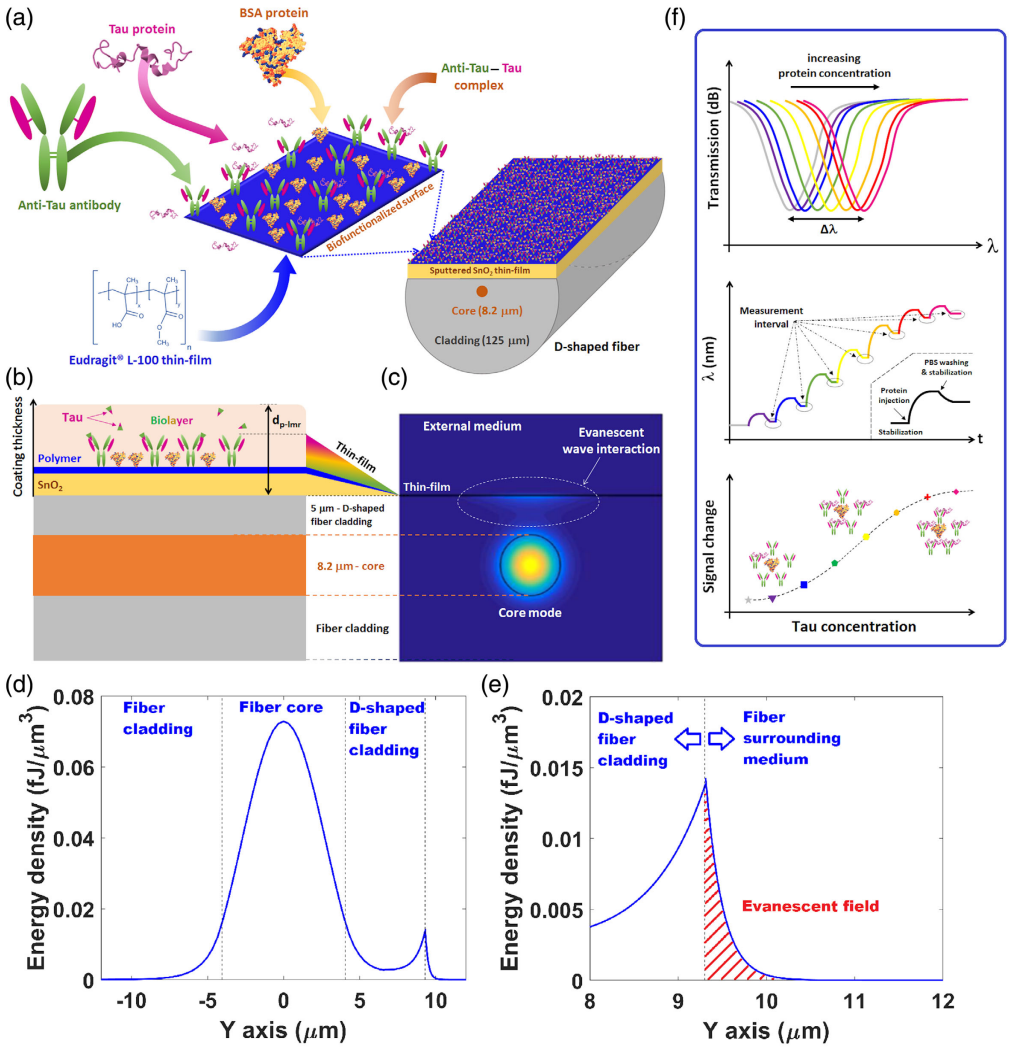

Figure 6. a) Sketch of the nanofunctionalized fiber sensors for the detection of Tau protein consisting of different elements: SnO_{2-x} nanocoating, Eudragit nanofunctional film, anti-Tau receptor, BSA surface passivator, and Tau analyte. b) Cross section of the structure and c) optical field intensity distribution of the core mode simulated with FIMMWAVE. d) Cross-sectional energy density of the electromagnetic wave of the core mode and e) related enlargement at the fiber/surrounding medium interface underlining the evanescent tail. f) Schematic of the real-time tracking of the spectral optical features at different stages of the biosensor assay, the wavelength shift of the LMR, and the biosensor dose–response curve.

purchased from Phoenix Photonics (UK), where a specific length of 17 mm of the fiber was progressively polished down until an attenuation of 1 dB at 1550 nm was attained in high RI matching oil (1.5 RIU).

According to previous literature,[21,31] a coating of around (160 ± 10) nm was deposited around the polished fiber portion. The procedure of coating deposition of the SnO_{2-x} thin film consisted of placing the fiber inside a DC sputter machine (K675XD from Quorum Technologies) at a partial pressure of argon of 9×10^{-2} mbar and a current intensity of 90 mA, and monitoring the LMR spectral features (i.e., resonance wavelength and visibility) while the coating was deposited. The thickness of the thin film was measured after the deposition.

Sensing System: The experimental setup employed to monitor and record the optical spectrum from the thin-film deposition up to the implementation of the biological assay is detailed in the **Figure 7**. The light is launched into the fiber by a multi-LED light source (Fibrelabs, Inc., SLD1310/1430/1550/1690). D-shaped fiber permits to separate the TE and TM components of an LMR. However, it turns out crucial to polarize the light in order to obtain a deeper resonance in the optical spectrum and hence to optimize the optical features of LMR.[26] Therefore, the in-line polarizer (Phoenix Photonics LTD) located between the light source and the fiber enables the polarization of light in one axis, while the following polarization controller rotates this axis in order to impinge light in the sensing region either at TE or TM polarization. The same can also be attained using a polarization maintaining fiber.[64] The output of the fiber is connected to an optical spectrum analyzer (OSA, MS9030A-MS9701B, Anritsu), which collects the optical spectrum and allows the measurement of the LMR resonance wavelength in the range of 1200–1700 nm with spectral resolution of 0.1 nm.

As shown in Figure 7, the nanofunctionalized fiber sensor is placed inside an ad hoc developed thermo-stabilized microfluidic system. The microfluidic system allows to handle small liquid samples in the order of tens of µL and at the same time to keep the temperature of the sensor stable during the whole assay. The microfluidic system consists of two equal-size pieces that can be assembled keeping a central flow channel with capacity for roughly 50 µL inside. The upper bar is made of polymethyl methacrylate (PMMA), which allows the visual inspection of the liquid flowing inside the flow channel, and the bottom one is made of stainless steel because has to guarantee the temperature adjusent avoiding any thermal fluctuation. Both are sealed with Parafilm R sheet interposed between the two parts to assure the water-proofing. For the mechanical stabilization of the fiber, the PMMA piece of the flow cell has two v-grooves (60° angle, 0.3 mm depth) engraved on both ends where the fiber is glued using an UV optical flexible adhesive (Norland 68) that polymerizes under UV light (Bondwand UV curing system, Electro-Lite) in a few minutes. In addition, the flow channel is connected to a peristaltic pump by means of a medical-grade PVC tubing (F117936; 0.76 mm inner diameter) used to inject the solutions into the microfluidic system. Finally, the temperature control system included two Peltier cells, which heat the stainless steel bar and then keep the microfluidic system at a constant temperature with a maximum error of ±0.05 °C, and a thermistor inserted into a lateral hole of this bar that provides the temperature feedback to the current-driven controlling unit (ILX Lightwave LDC-3722B TEC controller) to the Peltier cells. The temperature of the flow channel is measured by a thermocouple connected to a thermometric measuring unit (Lutron TM-917) and placed inside the PMMA bar as close as possible to the flow channel.

Chemical and Biological Reagents: The methacrylic acid/methacrylate copolymer (Eudragit L100) was provided by Evonik Health Care. 1-ethyl-3-(3-dimethylaminopropyl) carbodiimide hydrochloride (EDC), N-hydroxysuccinimide (NHS), and 6×-His Tag Monoclonal Antibody (AD1.1.10), HRP (Invitrogen) were purchased from Thermo Fisher Scientific. Ethanol (EtOH), PBS (40 mM, pH 7.4), BSA, EA, Tris HCl, SDS, 3,3′,5,5-tetramethylbenzidine (TMB), stop reagent for TMB substrate, PBS with 0.05% TWEEN 20 (pH 7.4), the Tau protein (Tau-441), and the corresponding high-affinity antibody anti-Tau (clone 46) were purchased from Sigma Aldrich Inc. Commercially available CSF was provided by Tocris Bioscience and the custom-made CSF components (NaCl 150 mM, KCl 2 mM, MgCl 6H2O 0.787 mM, $CaCl_2$ $2H_2O$ 1.42 mM, NaH_2PO_4 H_2O 1.52 mM, Glucose 13 mM, and Na2HPO4 7.74 mM) were purchased from Sigma Aldrich Inch. The human serum was acquired from HyTest Ltd.

Surface Functionalization and Tau Detection: The developed model assays require the suitable nanofunctionalization of optical fiber sensors, i.e., the D-shaped region. A thin layer (roughly 60 nm thick[21]) of the copolymer Eudragit L100 provides the free functionalities necessary for antibody immobilization on the sensor surface. For this purpose, the sensitive region of the fiber was immersed in 2 mM (0.04% w/v) Eudragit L100 in ethanol for 1 min and then left drying in air for 15 min.

After the copolymer deposition, the fiber was placed inside the thermo-stabilized microfluidic system. The temperature was fixed at

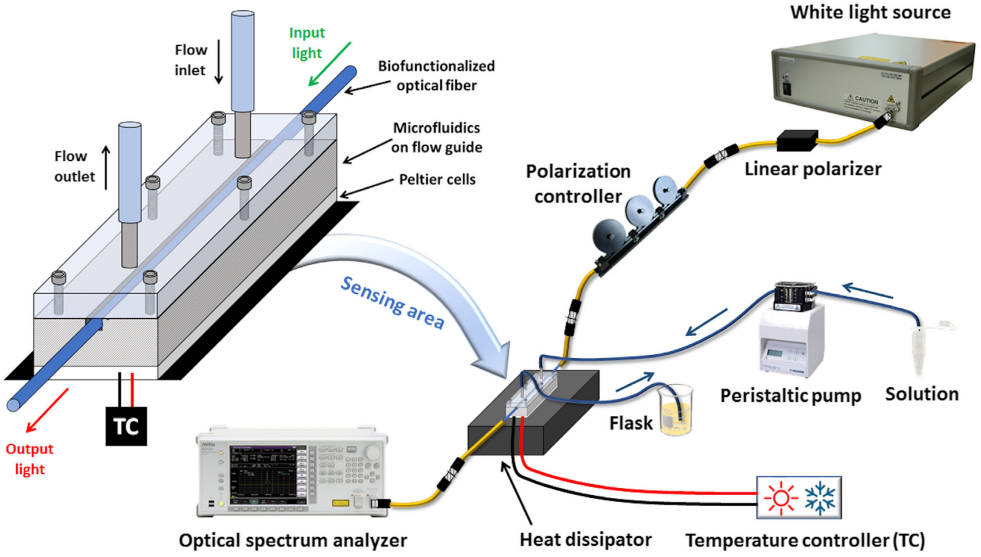

Figure 7. Complete experimental setup of the nanofunctionalized fiber sensors for the detection of biomolecules consisting of a custom-made microfluidic system, of a complete optical setup able to guide the light from a broadband source to the detector with controlled polarization conditions, and of a peristaltic pump for the injection of solutions into the microfluidic channel at controlled flow rates.

23 °C (±0.05 °C) during all the experiments, so roughly 2 °C below room temperature. This choice permits to avoid oscillations of the temperature controller system and hence to keep the temperature of the microfluidic system as stable as possible. The functional groups were activated by an EDC/NHS solution (2 mM/5 mM, respectively), which was injected at 12.6 μL min^{-1} for 20 min. This time is considered enough to guarantee proper activation of the functionalities. Afterward, to covalently graft the antibody, 200 μg mL^{-1} of Tau46 antibody in PBS solution was immediately injected for 1 h at a flow rate of 1.3 μL min^{-1}, followed by PBS rinsing for 10–15 min at a flow rate of 42 μL min^{-1} in order to remove unreacted antibodies. To complement the preparation of the sensing surface, in order to prevent nonspecific adsorption of biomolecules, different blocking agents were tested: 200 mM EA (7.4 pH) and 10 mM Tris–HCl, individually and in combination with BSA (Figure S3 and S4, Supporting Information). Finally, a solution of 0.1% w/v BSA in PBS was selected as the best blocking agent for the model assay used. BSA was injected for 20 min at 12.6 μL mL^{-1} to block the remaining active groups on the sensing surface. The preparation of sensing surface was then concluded with another PBS rinsing for 10–15 min at 42 μL min^{-1} flow rate. The value of the LMR signal at this point defines the starting baseline in the sensor response to subsequent analyte detection.

Before serially injecting the specific analyte, the negative control test (or simply the sensor specificity[23]) was performed. Different matrices were taken into account, ranging from human serum to different types of CSF (Supporting Information and Figure 5 and 7). In all cases, the solution was injected for 15–20 min at a flow rate of 3 μL min^{-1}. The assay was then completed by detecting increasing concentrations of Tau-441 ranging from 1 ng mL^{-1} up to 10 μg mL^{-1} and spiked in different CSF-based biofluids, following the same detection protocol: analyte injection for 15–20 min at a flow rate of 3 μL min^{-1}, subsequent PBS rinsing for 10–15 min at a flow rate of 42 μL min^{-1}, and then the measurement window at flow stopped for 10–15 min (to avoid any influence/interference due to temperature fluctuations, flow variation, and solution bulk effect). As the sensor is sensible to the different RI of the solutions, the PBS rinsing has the dual role of removing the remain of analytes as well as of measuring the real shift of the LMR signal (resonance wavelength) of each step caused by the antibody–analyte binding interaction.[23]

Biochemical Approaches for Protein Detection: As far as gel electrophoresis is concerned, Tau protein (Tau-441) in the range of 0.1–0.3 μg (8.3–25 μg mL^{-1}) was resuspended in 4× Laemmli buffer in the absence/presence of beta-mercaptoethanol. Protein material was separated by sodium dodecyl SDS-PAGE with 4–15% acrylamide and electrophoretically transferred to a nitrocellulose membrane in 7 min (up to 25 V) using a Trans-blot Turbo Transfer System (Bio-Rad). Ponceau staining was used to check protein loading.

For the immunodetection, membrane was probed with the anti-Tau antibody (clone 46) at 1:1000 dilution in 5% nonfat milk. After incubation with the appropriate horseradish peroxidase-conjugated secondary antibody (1:5000 dilution), the immunoreactivity was visualized by enhanced chemiluminescence (Perkin Elmer) and detected by a Chemidoc MP Imaging System (Bio-Rad).

ELISA used was based on an in-house assay with the aim to exclusively demonstrate the binding affinity of the selected antibody–antigen pair, i.e., Tau protein (Tau-441) and anti-Tau antibody (clone 46). Specifically, 1 μg mL^{-1} of the primary antibody was spiked in PBS. After that, the microplate was coated with 100 μL of the primary antibody solution per well, then covered and, finally, underwent overnight incubation at 4 °C. The remaining free functionalities were blocked with 200 μL of a commercial blocking buffer (Rockland) for 1 h at room temperature. Afterward, each column of the microplate was coated by different analyte concentrations (Tau-441–His protein) in the range of 0.0001–1 μg (0.0083–83 μg mL^{-1}) and then underwent incubation for 2 h at room temperature. Later, an extensive and repeated (three times) rinsing step with PBS-Tween 0.05% was carried out to remove unbound substances after each of the following three steps: injecting 1:500 PBS-diluted secondary antibody (6×-His Tag Monoclonal Antibody (AD1.1.10), HRP) that binds to the immobilized Tau-441–His protein and incubating for 1 h at room temperature; adding 100 μL per well of HRP substrate TMB for the detection of bound protein; stopping the reaction after 30 min by adding 100 μL per well of stop reagent for TMB substrate and, finally, reading the plate at 450 nm in a microplate reader.

Supporting Information

Supporting Information is available from the Wiley Online Library or from the author.

Acknowledgements

F.C. and D.S.R. contributed equally to this work. A.G. and I.R.M. considered equally as last author in this work. F.C. gratefully acknowledges the support of the National Research Council of Italy (CNR) for the Short-Term Mobility programs 2017 and 2019. I.D.V. and I.R.M. acknowledge partial support of the Spanish Ministry of Economy and Competitiveness (Nos. TEC2016-79367-C2-2-R and PID2019-106231RB-I00), the predoctoral research grants of the Public University of Navarra and the Public University of Navarra grant PJUpna1936. E.S. and J.F-I. acknowledge partial support of the Spanish Ministry of Science, Innovation and Universities (PID2019-110356RB-I00/AEI/10.13039/501100011033). T.G. gratefully acknowledges the support of the National Natural Science Foundation of China (Nos. 62035006, 61975068, and 62011530459), the Guangdong Outstanding Scientific Innovation Foundation (No. 2019TX05X383), and the Program of Marine Economy Development Special Fund (Six Marine Industries) under Department of Natural Resources of Guangdong Province (No. GDNRC [2021]33).

Conflict of Interest

The authors declare no conflict of interest.

Data Availability Statement

The data that support the findings of this study are available from the corresponding author upon reasonable request.

Keywords

Alzheimer's disease, biophotonic platforms, lossy-mode resonances, microfluidics, nanofunctionalized optical fibers

Received: February 22, 2022
Revised: May 5, 2022
Published online: July 18, 2022

[1] G. Chene, A. Beiser, R. Au, S. R. Preis, P. A. Wolf, C. Dufoil, R. Seshadri, *Alzheimers Dement.* **2015**, *16*, 310.
[2] M. Prince, A. Wimo, M. Guerchet, G. C. Ali, Y. T. Wu, M. Prina, *Alzheimer's Disease International. World Alzheimer Report 2015. The Global Impact of Dementia. An analysis of prevalence, incidence, costs, and trends. World Alzheimer's Report.*
[3] M. Waser, T. Benke, P. Dal-Bianco, H. Garn, J. A. Mosbacher, G. Ransmayr, R. Schmidt, S. Seiler, H. B. D. Sorensen, P. J. Jennum, *Brain Behav.* **2019**, *9*, 01197.
[4] N. J. Ashton, A. Leuzy, T. K. Karikari, A. Dodich, M. Boccardi, H. Barthel, G. N. Bischof, M. C. Carrillo, K. Chiotis, J. Corre, J.-F. Démonet, A. Drzezga, A. F. Gietl, K. C. Johnson, M. Lorenzi, A. K. Nordberg, R. Ossenkoppele, G. D. Rabinovici, O. Ratib, O. Sabri, V. Treyer, P. G. Unschuld, V. L. L. Villemagne,

B. Winblad, E. E. Wolters, G. B. Frisoni, V. Garibotto, N. Mattsson, H. Zetterberg, K. Blennow, et al., *Alzheimer's Dement.* **2020**, *16*, 039557.
[5] B. Olsson, R. Lautner, U. Andreasson, A. Ohrfelt, E. Portelius, M. Bjerke, M. Hölttä, C. Rosén, C. Olsson, G. Strobel, E. Wu, K. Dakin, M. Petzold, K. Blennow, H. Zetterberg, *Lancet Neurol.* **2016**, *15*, 673.
[6] E. Lawrence, C. Vegvari, A. Ower, C. Hadjichrysanthou, F. De Wolf, R. M. Anderson, *J. Alzheimer's Dis.* **2017**, *59*, 1359.
[7] R. A. Huynh, C. Mohan, *Front. Neurol.* **2017**, *8*, 102.
[8] L. Zhu, Q. Yuan, Z. Zeng, R. Zhou, R. Luo, J. Zhang, C. K. Tsang, W. Bi, *J. Alzheimers Dis.* **2021**, *79*, 1171.
[9] A. Dodich, M. Boccardi, N. J. Ashton, H. Barthel, G. N. Bischof, M. C. Carrillo, K. Chiotis, J. Corre, J.-F. Démonet, A. Drzezga, A. F. Gietl, O. Hansson, K. A. Johnson, A. Leuzy, M. Lorenzi, A. K. Nordberg, R. Ossenkoppele, G. D. Rabinovici, O. Ratib, O. Sabri, V. Treyer, P. G. Unschuld, V. L. L. Villemagne, B. Winblad, E. E. Wolters, G. B. Frisoni, V. Garibotto *Alzheimer's Dement.* **2020**, *16*, 039549.
[10] M. Goedert, M. G. Spillantini, R. Jakes, D. Rutherford, R. A. Crowther *Neuron* **1989**, *3*, 5195.
[11] K. Iqbal, F. Liu, C. X. Gong, I. Grundke-Iqbal, *Curr Alzheimer Res.* **2010**, *7*, 656.
[12] Z. Yan, S. Jianhua, C. Dandan, W. Hu, Z. Guan, C.-X. Gong, K. Iqbal, F. Liu, *Front. Aging Neurosci.* **2018**, *10*, 27.
[13] K. Blennow, H. Zetterberg, *J. Intern. Med.* **2018**, *284*, 643.
[14] K. Kim, M.-J. Kim, D. W. Kim, S. Y. Kim, S. Park, C. B. Park, *Nat. Commun.* **2020**, *2*, 119.
[15] C. R. Jack, D. A. Bennett, K. Blennow, M. C. Carrillo, H. H. Feldman, G. B. Frisoni, H. Hampel, W. J. Jagust, K. A. Johnson, D. S. Knopman, R. C. Petersen, P. Scheltens, R. A. Sperling, B. Dubois, *Neurology* **2016**, *87*, 539.
[16] J. Cummings, G. Lee, A. Ritter, M. Sabbagh, K. Zhong, *Alzheimers Dement.* **2019**, *5*, 272.
[17] T. Pan, D. Lu, H. Xin, B. Li, *Light Sci. Appl.* **2021**, *10*, 124.
[18] N. Toropov, G. Cabello, M. P. Serrano, R. R. Gutha, M. Rafti, F. Vollmer, *Light Sci. Appl.* **2021**, *10*, 42.
[19] L. Liu, X. Zhang, Q. Zhu, K. Li, Y. Lu, X. Zhou, *Light Sci. Appl.* **2021**, *10*, 181.
[20] C. Caucheteur, T. Guo, F. Liu, B.-O. Guan, J. Albert, *Nat. Commun.* **2016**, *7*, 13371.
[21] F. Chiavaioli, P. Zubiate, I. Del Villar, C. R. Zamarreño, A. Giannetti, S. Tombelli, C. Trono, F. J. Arregui, I. R. Matias, F. Baldini, *ACS Sens.* **2018**, *3*, 936.
[22] M. Janik, S. V. Hamidi, M. Koba, J. Perreault, R. Walsh, W. J. Bock, M. Smietana, *Lab Chip* **2021**, *21*, 397.
[23] F. Chiavaioli, C. Gouveia, P. Jorge, F. Baldini, *Biosensors* **2017**, *7*, 23.
[24] J. Lao, P. Sun, F. Liu, X. Zhang, C. Zhao, W. Mai, T. Guo, G. Xiao, J. Albert, *Light Sci. Appl.* **2018**, *7*, 34.
[25] P. Vaiano, B. Carotenuto, M. Pisco, A. Ricciardi, G. Quero, M. Consales, A. Crescitelli, E. Esposito, A. Cusano, *Laser Photonics Rev.* **2016**, *10*, 922.
[26] F. Chiavaioli, D. Janner, *J. Lightwave Technol.* **2021**, *39*, 3855.
[27] I. Dominguez, I. Del Villar, O. Fuentes, J. M. Corres, I. R. Matias, *Sci. Rep.* **2021**, *11*, 3669.
[28] O. Fuentes, I. Del Villar, J. M. Corres, I. R. Matias, *Sci. Rep.* **2019**, *9*, 8882.
[29] A. Socorro-Leránoz, D. Santano, I. Del Villar, I. R. Matias, *Biosens. Bioelectron. X* **2019** *1*, 100015.
[30] F. Esposito, L. Sansone, A. Srivastava, F. Baldini, S. Campopiano, F. Chiavaioli, M. Giordano, A. Giannetti, A. Iadicicco, *Biosens. Bioelectron.* **2021**, *172*, 112747.
[31] P. Zubiate, A. Urrutia, C. R. Zamarreño, J. Egea-Urra, J. Fernández-Irigoyen, A. Giannetti, F. Baldini, S. Díaz, I. R. Matias, F. J. Arregui, E. Santamaría, F. Chiavaioli, I. D. Villar *Biosens. Bioelectron. X* **2019**, *2*, 100026.
[32] M. J. Pollitt, G. Buckton, R. Piper, S. Brocchini, *RSC Adv.* **2015**, *5*, 24521.
[33] A. Frutiger, A. Tanno, S. Hwu, R. F. Tiefenauer, J. Vöros, N. Nakatsuka, *Chem. Rev.*, **2021**, *121*, 8095.
[34] I. Del Villar, F. J. Arregui, C. R. Zamarreño, J. M. Corres, C. Bariain, J. Goicoechea, C. Elosua, M. Hernaez, P. J. Rivero, A. B. Socorro, A. Urrutia, P. Sanchez, P. Zubiate, D. Lopez, N. De Acha, J. Ascorbe, I. R. Matias, *Sens. Actuators B Chem.* **2017**, *240*, 174.
[35] R. Wang, X. Zhou, X. Zhu, L. Liu, H. Shi, *ACS Sens.* **2017**, *2*, 257.
[36] T. M. Squires, R. J. Messinger, S. R. Manalis, *Nat. Biotechnol.* **2008**, *26*, 417.
[37] J. Robinson, D. Roush, S. M. Cramer. *J. Chromatogr. A.* **2020**, *1617,* 460838.
[38] F. Waibl, M. L. Fernández-Quintero, A. S. Kamenik, J. Kraml, F. Hofer, H. Kettenberger, G. Georges, K. R. Liedl. *Biophys. J.* **2021**, *120*, 143.
[39] J. Tu, P. Bennett, *Bioanalysis*, **2017**, *9*, 1107.
[40] K. Blennow, A. Wallin, H. Ågren, C. Spenger, J. Siegfried, E. Vanmechelen, *Mol. Chem. Neuropathol.* **1995**, *26*, 231.
[41] L. Grangeon, C. Paquet, S. Bombois, M. Quillard-Muraine, O. Martinaud, B. Bourre, R. Lefaucheur, G. Nicolas, J. Dumurgier, E. Gerardin, M. Jan, J.-L. Laplanche, K. Peoc'h, J. Hugon, F. Pasquier, D. Maltête, D. Hannequin, D. Wallon, *J Alzheimers Dis.* **2016**, *51*, 905.
[42] R. A. Dudley, P. Edwards, R. P. Ekins, D. J. Finney, I. G. McKenzie, G. M. Raab, D. Rodbard, R. P. Rodgers, *Clin Chem.* **1985**, *31*, 1264.
[43] R. Karlsson, P. S. Katsamba, H. Nordin, E. Pol, D. G. Myszka, *Anal. Biochem.* **2006**, *349*, 136.
[44] Analytical Methods Committee *Analyst* **1987**, *112*, 199.
[45] M. Goedert, R. Jakes, *EMBO J.* **1990**, *9*, 4225.
[46] B. Penke, M. Szűcs, F. Bogár, *Molecules* **2020**, *25*, 1659.
[47] Y. Shi, W. Zhang, Y. Yang, A. G. Murzin, B. Falcon, A. Kotecha, M. van Beers, A. Tarutani, F. Kametani, H. J. Garringer, R. Vidal, G. I. Hallinan, T. Lashley, Y. Saito, S. Murayama, M. Yoshida, H. Tanaka, A. Kakita, T. Ikeuchi, A. C. Robinson, D. M. A. Mann, G. G. Kovacs, T. Revesz, B. Ghetti, M. Hasegawa, M. Goedert, S. H. W. Scheres, *Nature* **2021**, *598*, 359.
[48] A. Lahav, M. Auslender, I. Abdulhalim, *Opt. Lett.* **2008**, *33*, 2539.
[49] F. J. Arregui, I. Del Villar, C. R. Zamarreño, P. Zubiate, I. R. Matias, *Sens. Actuators B Chem.* **2016**, *232*, 660.
[50] T. K. Karikari, A. Emeršič, A. Vrillon, J. Lantero-Rodriguez, N. J. Ashton, M. G. Kramberger, J. Dumurgier, C. Hourregue, S. Čučnik, G. Brinkmalm, U. Rot, H. Zetterberg, C. Paquet, K. Blennow. *Alzheimer's Dement.* **2021**, *17,* 755.
[51] C. Wattmo, K. Blennow, O. Hansson. *BMC Neurol.* **2020**, *20,* 10.
[52] K. Hansson, R. Dahlén, O. Hansson, E. Pernevik, R. Paterson, J. M. Schott, N. Magdalinou, H. Zetterberg, K. Blennow, J. Gobom. *Clin. Mass Spectrometry* **2019**, *14,* 74.
[53] D. Galasko, M. Xiao, D. Xu, D. Smirnov, D. P. Salmon, N. Dewit, J. Vanbrabant, D. Jacobs, H. Vanderstichele, E. Vanmechelen, P. Worley. *Alzheimer's Dement.* **2019**, *5,* 871.
[54] M. Riemenschneider, S. Wagenpfeil, H. Vanderstichele, M. Otto, J. Wiltfang, H. Kretzschmar, E. Vanmechelen, H. Förstl, A. Kurz. *Mol. Psychiatry* **2003**, *8,* 343.
[55] T. Sunderland, G. Linker, N. Mirza, K. T. Putnam, D. L. Friedman, L. H. Kimmel, J. Bergeson, G. J. Manetti, M. Zimmermann, B. Tang, J. J. Bartko, R. M. Cohen *JAMA* **2003**, *289*, 2094.
[56] X. Chen, Y. Liu, J. Huang, W. Liu, J. Huang, Y. Zhang, W. Fu, *Front. Lab. Med.* **2017**, *1*, 82-.
[57] T. T. Vu Nu, N. H. T. Tran, E. Nam, T. T. Nguyen, W. J. Yoon, S. Cho, J. Kim, K.-A. Chang, H. Ju *RCS Adv.* **2018**, *8*, 7855.

[58] I. Ziu, E. T. Laryea, F. Alashkar, C. G. Wu, S. Martic, *Anal. Bioanal. Chem.* **2020**, *412*, 1193.
[59] M. Vestergaard, K. Kerman, D.-K. Kim, H. M. Hiep, E. Tamiya, *Talanta* **2008**, *74*, 1038.
[60] D. Li, M. M. Mielke, *Neurol. Ther.* **2019**, *8*, 73.
[61] X.-L. Ding, Q. Z. Tuo, P. Lei, *J Alzheimers Dis.* **2021**, *80*, 1353.
[62] I. Del Villar, C. R. Zamarreño, M. Hernaez, F. J. Arregui, I. R. Matias, *Opt. Express* **2010**, *18,* 20183.
[63] S. P. Usha, S. K. Mishra, B. D. Gupta, *Sens. Actuators B: Chem.* **2015**, *218,* 196.
[64] A. Andreev, B. Pantchev, P. Danesh, B. Zafirova, E. Karakoleva, E. Vlaikova, E. Alipieva, *Sens. Actuators B: Chem.* **2005**, *106,* 484.